Sound localization in the lizard using internally coupled ears : a finite-element approach

Reference:
Livens Pieter, Muyshondt Pieter, Dirckx Joris.- Sound localization in the lizard using internally coupled ears : a finite-element approach
Hearing research - ISSN 0378-5955 - Amsterdam, Elsevier science bv, 378(2019), p. 23-32
Full text (Publisher's DOI): https://doi.org/10.1016/J.HEARES.2019.01.016
To cite this reference: https://hdl.handle.net/10067/1612930151162165141

Sound localization in the lizard using internally coupled ears: a finite-element approach

Pieter Livens[a,1], Pieter G.G. Muyshondt[a], Joris J.J. Dirckx[a]

[a]*Biophysics and Biomedical Physics, University of Antwerp, Groenenborgerlaan 121, 2020 Antwerp, Belgium*

[1]*E-mail address: pieter.livens@uantwerpen.be*

Abstract

A number of interesting differences become apparent when comparing the hearing systems of terrestrial vertebrates, especially between mammals and non-mammals. Almost all non-mammals possess only a single ossicle, enabling impedance matching and hearing below 10 kHz. The middle ear (ME) evolved as a chain of three ossicles in mammals, enabling sound transmission up to higher frequencies than in similar-sized non-mammals. The relatively low-frequency hearing in non-mammals is associated with audible wavelengths that are significantly larger than the head. Therefore, it is unlikely that localization of the sound source can be obtained by using external cues between the ears (intensity and time difference between both sides), especially when compared to similarly sized mammals. The heads of many non-mammals contain large air-filled cavities, which acoustically couple both MEs. This article studies acoustic responses and sound-source localization capabilities of the coupled MEs of the brown anole (*Anolis sagrei*), using finite-element modeling. Based on high-resolution μCT data, 3D finite-element models of the ME and interaural cavity were constructed. The parameter values in the ME model were determined such that the response of the isolated ME matches experimental data of literature and the velocity ratio between the tympanic membrane (apex) and footplate reflects the anatomical arrangement of the columellar lever in the anole. It was found from simulation of the coupled ME model that the interaural connection amplifies intensity differences between both sides and thus enhances the capability of sound-source localization. In addition, the interaural canal doubles the phase differences of the incident external sound waves between the eardrums. In isolated ears, generating such phase differences would require head sizes twice as large. Effects of the inner-ear loading on the sound-source localization of the coupled MEs were investigated as well. The inner-ear load lowered the peak velocity ratios between the ears, but created broader plateaus of useful directionality, indicating that inner-ear loading not only influences sound perception but also sound localization in internally connected ears.

Keywords

Lizard middle ear, brown anole, interaural coupling, directional hearing, finite-element modeling.

Highlights

- Interaural coupling in the anole lizard was studied using 3D FE modeling
- The interaural cavity amplifies directional cues, both for amplitude and phase
- Inner-ear loading lowers the amplitude cues, but broadens the directional bandwidth

Abbreviations

(µ)CT, (micro) computed tomography; BC, boundary condition; CL, contralateral; FE, finite element; FP, footplate; IE, inner ear; IL, ipsilateral; ILD, interaural level difference; ITD, interaural time difference; ME, middle ear; PI, pars inferior; PS, pars superior; SPL, sound pressure level; TM, tympanic membrane

1. Introduction

For all animals, hearing and localizing sound are of great importance in their daily functioning. The middle ear (ME) developed independently among the ancestors of mammals, frogs, reptiles and birds, resulting in the diverse set of MEs found in nature (Manley, 2010; Grothe and Pecka, 2014). The ME consists of the eardrum (tympanic membrane; TM) and one or multiple ME ossicles, and functions to bridge the acoustic impedance difference between air and the fluids of the inner ear (IE) to prevent acoustic energy from being reflected at the interface. Mammals rely on three ossicles to efficiently transfer audible airborne pressure waves to the IE by air conduction. In non-mammalian terrestrial vertebrates, one finds only a single ossicle: *the columella* (e.g., in reptiles (Wever, 1978) and in birds (Muyshondt et al., 2016b)). The pressure amplification from the TM to the footplate (FP) by the ME system is mainly determined by the area ratio of TM to FP and by the lever ratio of the ME (Saunders et al., 2000). This lever in lizards is determined by the location of connection of the (extra)columella on the TM (see Fig. 1B, yellow lines). Since the motions on the TM apex are larger than on the connection point with the (extra)columella, force amplification is acquired. This simplified single-ossicle setup in non-mammals does not preclude good hearing. For example, many lizards have hearing ranges between 0.1-8 kHz (Brittan-Powell et al., 2010; Dooling et al., 2000), roughly matching the lower half of the human hearing range. Within their respective frequency range of best hearing, lizards (and more notably birds) have cochlear sensitivities similar to that of humans (Manley, 2017; Manley and Köppl, 1998), so MEs utilizing one or three ossicles appear equally efficient in the overlapping hearing ranges.

In mammals, the narrow Eustachian tubes only open when swallowing, mainly to equalize the pressure between the medial and lateral sides of the TM. The ME cavity has no other pathways or openings inside the skull. Mammalian MEs are therefore acoustically isolated from each other since, no possible internal pathway for sound exists between the ears on both sides. This implies that differences in TM vibration between both ears can only be created by externally originated differences in sound pressure. These interaural level differences (ILDs) and interaural time differences (ITDs) of the sound signal between the ears provide directional information of the sound source. The ILDs occur due to "acoustic shadow" of the head, and the ITDs are mainly caused by the finite travel time of the pressure wave around the head. The ILDs and ITDs are therefore strongly dependent on the animal's head size and audible frequency range. Localization of a sound source with ILDs and ITDs is presumed to be difficult in the case that the head size is small relative to the wavelength of the sound in the audible frequency range. In contrast, the ME cavities of non-mammals (including many reptile and bird species) are connected by very wide "Eustachian tubes" via the mouth cavity and/or an interaural canal[1] (Christensen-Dalsgaard, 2011; Wever, 1978; Young, 2016). When a sound wave induces motion of one TM from the lateral side, the TM vibrations will generate a partially attenuated internal pressure wave through the internal connection. In non-mammals, these waves are able to propagate through the connecting cavity, reach the other TM on the medial side and influence its vibration amplitude and phase by altering the instantaneous pressure difference across the TM. The wave propagation via the internal cavity enables the TMs of non-mammals to function as pressure-gradient receivers. Non-mammals use these gradients to create binaural cues at the level of the TM, contrary to mammals which rely exclusively on external pressures and the subsequent neural processing between the TM signals (Christensen-Dalsgaard, 2011; Köppl, 2009).

In lizards, a strong directionality is observed, with up to 40 dB differences between ipsi- and contralateral stimulation; i.e., when the sound source is placed laterally to one of the TMs, one meter from the head (Christensen-Dalsgaard, 2011; Christensen-Dalsgaard and Manley, 2008). Optimal hearing frequencies of these animals range between 1-3 kHz. The corresponding wavelengths (34-11 cm) of sound are much larger than the head size of the animals (<1 cm), so it is improbable that the strong sense of sound-source localization can be achieved from only the ILDs and ITDs generated by the head. The strong directionality observed in experiments (e.g., Christensen-

[1] Note that some birds, notably owls, have acoustically isolated MEs, although anatomically there is an interaural connection to be found (Christensen-Dalsgaard and Manley, 2005).

Dalsgaard, 2011; Christensen-Dalsgaard and Manley, 2008) is therefore presumed to be enhanced by the internal interaural connection between the MEs on both sides. Although experiments demonstrate a clear directionality in lizards, and thus suggest a contribution of the internal connection to the directionality, investigating the mechanisms of how the interaural canal contributes to localization is still an ongoing process. Furthermore, no model with accurate anatomy for directional hearing currently exists, although some models with simplified geometries have been used to describe directional hearing by means of the internal interaural connection (Fletcher, 1992; Christensen-Dalsgaard and Manley, 2005, 2008; Vossen et al., 2010; Vedurmudi et al., 2016a, 2016b).

To invest on directionality of the lizard species with a single-ossicle ME, we built a 3D finite element (FE) model of the MEs and the interaural cavity of a brown anole (*Anolis sagrei*). This lizard species has a single-ossicle ME (Wever and Werner, 1970), and showed clear directionality (Christensen-Dalsgaard and Manley, 2008). The parameter values in the model were determined such that the responses of the uncoupled ME model under acoustic TM stimulation matched experimental data from Christensen-Dalsgaard and Manley (2008). Subsequently, we studied the coupled ME model to deduce the directionality in the anole and how the ME and interaural cavity play a role in the acoustical coupling of the TMs. Additionally, we investigated the effect of IE loading by applying a pressure load to the footplate (FP), utilizing a three-parameter model after Muyshondt et al. (2016a, 2018).

2 Materials and Methods

2.1 Morphology

To gather precise anatomical data of the coupled ear system, we utilized the µCT (micro computed tomography) scanning facilities of the Hercules group at the University of Brussels (VUB). The head of a male brown anole was scanned with a Skyscan 1172 µCT scanner. The fresh-frozen specimen was thawed and subsequently stained to increase soft tissue contrast. Staining was done for two days using 2.5% phosphotungstic acid (PTA) in daily refreshed deionized water to optimize contrast with minimal tissue shrinking (Buytaert et al., 2014). During scanning, the sample was stored in Parafilm (Bemis NA, Neenah, WI, USA) to prevent drying of the sample. The scanner used a source voltage of 70 kV and a source current of 141 µA. The total scan time was 3 hours and 23 minutes. After image reconstruction, the data set consisted of 2488 x 2568 x 2736 cubic voxels with a voxel size of 3.97 µm. On these data image segmentation was performed in Amira 6.3 (FEI Visualization Sciences Group, Hillsboro, OR, USA). Mostly automatic methods (seed filling and interpolation) were used, but manual intervention was needed to correctly detect boundaries of soft tissue structures. After segmentation, the combined geometry of the individual ME components and the interaural cavity was converted into a closed surface model of triangular elements. Smoothing and reducing the number of triangles was performed in Amira to minimize noise and to build a computationally practical model. From Amira we exported the surface model as an STL (Standard Tessellation Language) file to FE software (COMSOL Multiphysics 5.2, Burlington, MA, USA).

Figure 1 shows the final segmented geometry. In Fig. 1A the ME system of the anole is shown. The columella (purple) is medially supported by an annular ligament (pink) surrounding the FP and laterally by the internal process (yellow). The internal process connects and supports the columella and the extracolumella (green). The role of the internal process seems to be purely structural and may help to protect against head movements while chewing, since cutting it loose from the base in the skull does not alter the ME transfer function significantly (Saunders et al., 2000). The extracolumella connects to the fibrous middle layer of the TM (red) by means of three processes. The pars inferior (PI) process connects to the apex of the TM, and the pars superior (PS) process attaches to the rim of the TM. The posterior process could not be identified as a separate structure in the CT scans and is included in the structure of the PS. The extracolumellar and intratympanic ligament could not be identified in the scans and were therefore not included in the models. For more information on the anatomy of MEs in lizards we refer to Wever and Werner (1970) or the comparative review of Saunders et al. (2000). The midway attachment of the extracolumella on the processes on the TM determines the lever action of the ME. This lever is illustrated in Fig. 1B by the (yellow) line starting from the proximal end of the PI – at the TM apex – running over the PS back to the extracolumella. The location of the connection of the extracolumella on the processes allows for pressure amplification by a lever mechanism similar to a wheelbarrow. This second-order lever is universally present in other lizards, mammals and birds (Mason and Farr, 2013). For the anole, the fulcrum of the lever is located at the superior end of the pars superior. Since the angular velocity at the fulcrum is assumed the same for both lever arms, the lever ratio (l_1/l_2) is interchangeable with the velocity ratio (v_1/v_2); see the inset of Fig. 1B. Both *lever ratio* and *velocity ratio* will therefore be used interchangeably. Also illustrated in Fig. 1B is the ME surface mesh used in the models. Figures 1C and 1D show the encompassing interaural cavity (light blue). Figure 1C shows half of the interaural cavity as transparent to illustrate how the ME is orientated inside this structure.

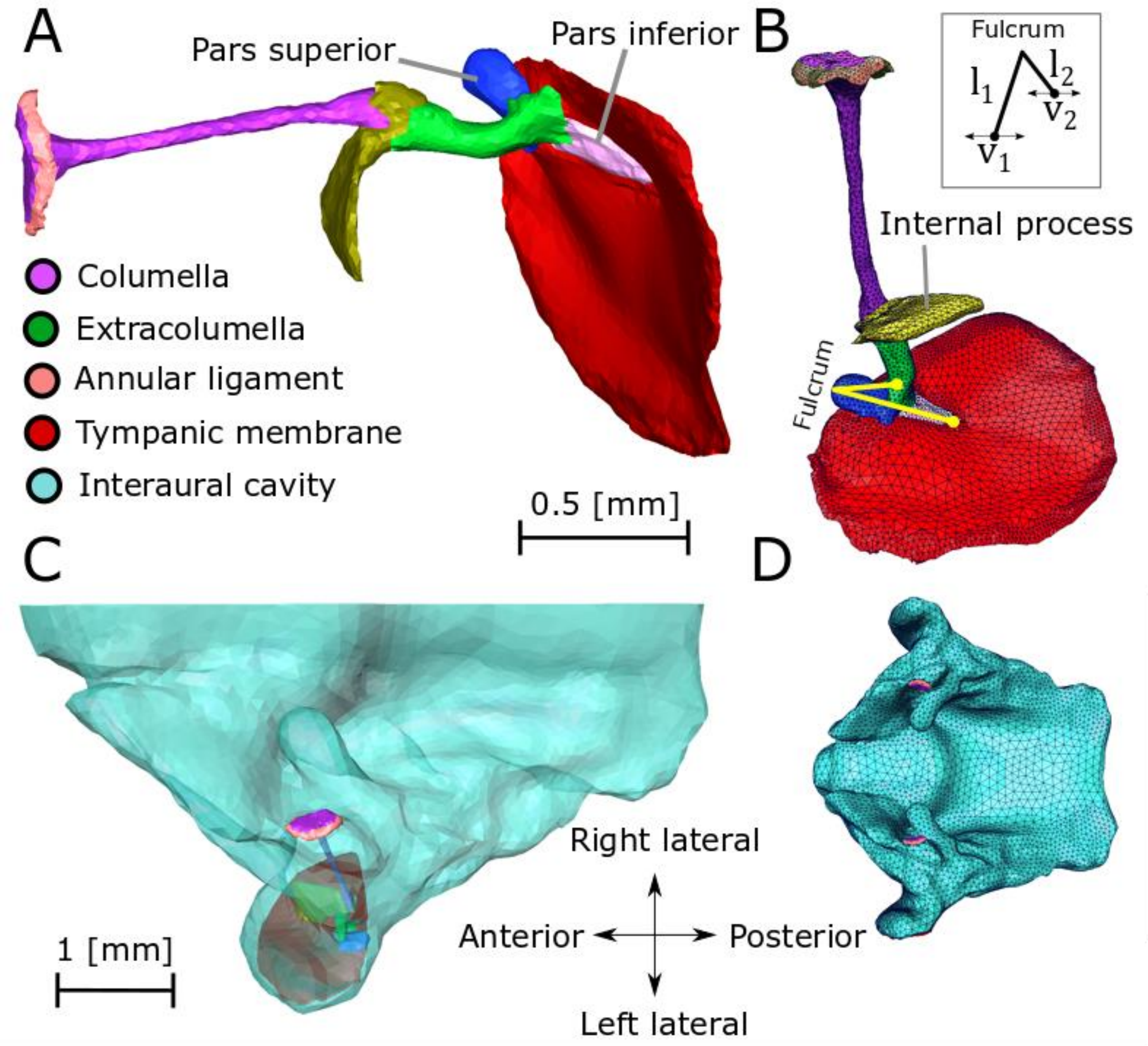

Figure 1. Geometry of the ME system in the brown anole used in the simulations. (A and B) The single-ossicle ME of the anole is described by a surface triangulation (see section 3.1), which can be used as geometric input for FE calculations. The three major processes are labeled, while other major structures are indicated in the color legend. The posterior process could not be separately identified and is included in the PS. In Fig. 1B, the lever formed by the columellar attachment on the TM is illustrated by the yellow lines. The inset of Fig. 1B schematically illustrates the lever arms l_1 and l_2 and the corresponding velocities v_1 and v_2 (see text). (C) The head of the anole connects both MEs by a broad air-filled cavity. The cavity is made transparent to show the orientation of the ME relative to the body axes. Only the medial side of the footplate and annular ligament and the lateral side of the TM are not contained within the cavity. (D) The full model and the corresponding surface triangulation.

2.2 FE model description

2.2.1 The isolated ME model

We first focused on modeling of the isolated ME, without any interaction with the cavity and the contralateral ear, to estimate the parameter values in the ME model in comparison with experimental behavior of the ME in literature. The FE model describes all structures as quadratic tetrahedral solid elements, except for the thin TM for which a *shell* (surface) description was used, using quadratic triangular elements. Modeling the thin TM using tetrahedral solid elements instead, produces very skew elements with a high area-to-volume ratio, which results in poor computational accuracy and efficiency. Therefore, we modeled the medial surface of the TM as a shell on which pressure waves were applied, and which also incorporates bending moments of the TM. Using the method of Van der Jeught et al. (2013) the full-field thickness map of the TM was reconstructed using the original segmentation of the CT data. In the FE model this map is defined on the TM shell surface to implement the intrinsic thickness distribution of the membrane.

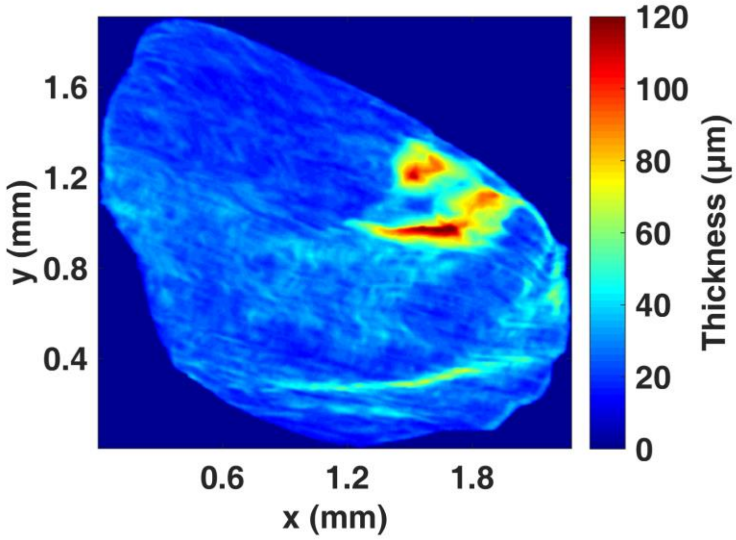

Figure 2. Thickness distribution of the TM of the anole. The thickness is largest where the PI attaches to the TM. The average thickness was calculated to be 28 µm. Values are constrained between [0, 120] µm for a better visual comparison between thick and thin regions.

Fig. 2 shows the TM thickness distribution derived from the described method. The thickness is relatively constant over the membrane and has an average value of 28 µm. The thickness of the TM is largest near the locations where the processes of the ME attach to the TM, but the precise thickness at the attachments is difficult to determine due to the connection with the other structures. The asymmetrical attachment of the processes to the

TM help with generating a broad frequency response (Fay et al., 2006) and the added thickness influences the TM stiffness and response (Koike et al., 2001).

The surrounding edge of the TM connects to different structures, consisting of different material properties, which possibly introduces different boundary conditions (BCs). All these connections fundamentally play a supporting role, giving stability to the TM while preserving TM mobility. The model used a simply-supported BC, allowing rotation but no displacement of the TM edge. For the support of the annular ligament and the internal process, neither displacements nor rotations were allowed, corresponding to a fully-clamped BC. On the annular ligament, the BC was applied to a set of edges forming a ring running around this ligament. For the internal process, a set of edges was selected where it attaches to the cavity bone (see Fig. 1C). Other BCs were tested, but these alterations have little effect on the total system response.

The model calculations were performed in the frequency domain, resulting in steady-state response of the ME at a series of individual frequencies. A uniform harmonic load of 1 Pa amplitude (94 dB SPL) was used as input on the TM. One of the largest uncertainties in modeling of these biomechanical systems rests on the material parameters of the anatomical components. The parameter values were estimated based on anatomical considerations, experimental data, or values used in other models. The anatomy in Fig. 1 indicates that a lever or velocity ratio of around 2 is expected in the ME of the anole, since the extracolumella attaches midway on the processes. For the annular ligament, a value of 0.145 MPa was adopted to give reasonable velocity ratios. This value was taken from literature (Muyshondt et al., 2018) and is based on the measured acoustic stiffness impedance of the annular ligament in ostrich (Muyshondt et al., 2016a). Given the data of Christensen-Dalsgaard and Manley (2008), maximal TM-apex velocities and corresponding resonance frequencies should be observed between 3-4.5 kHz. For the elasticity of the TM, a value of 4 MPa fulfilled the requirement of the resonance at 3-4.5 kHz, so this value was subsequently used in our model. We found that the Young’s modulus of the TM had the largest influence on the system response, which is consistent with the findings of previous work on the single-ossicle ear in duck (Muyshondt et al., 2016a). The influence of other structures and material properties were tested, but these changes had much smaller effect on system response.

Table 1. Material parameter values used in the ME model. Materials were treated as viscoelastic and modeled in the frequency domain, using a complex modulus $E' = E(1 + i\eta)$, except for the bony columella which was treated as purely elastic. ρ is the mass density, E is the Young's modulus, η is the damping loss factor and ν is Poisson's ratio. Material values were taken from [a] Muyshondt et al. (2016b) and [b] Muyshondt et al. (2018), except for the elasticity of the TM, which was adopted to better match the system response to literature values.

Component	ρ [10^3 kg/m^3]	E [MPa]	η	ν
TM	1.1	4	0.2	0.3
Extracolumella[a]	1.1	39.2	0.2	0.3
Columella[a]	2.2	14100	0	0.3
Annular lig.[b]	1.1	0.145	0.2	0.3
Internal process[a]	1.1	20	0.2	0.3

2.2.2 The inner ear

In many animals (including lizards) the IE plays an important and active role in ME motion (Manley, 2017). To include IE loading in the FE model, we followed the approach from Muyshondt et al. (2016a, 2018). The IE impedance Z_{IE} on the medial FP surface is a complex quantity, which was described by a three-parameter model

$$Z_{IE} = R + i(M \cdot \omega - K/\omega),$$

with M the acoustical mass, K the acoustical stiffness and R the acoustical damping. This description provided a good fit up until 4 kHz for the IE impedance amplitude in the ostrich, although the experimental phase was not optimally fitted by the model. Acoustical and mechanical variables are related by the area (A) squared (e.g., to transform mechanical mass (m) to acoustical mass (M) one uses: $M = m/A^2$). As a first estimation, the values from Muyshondt et al. (2016a) for K, M and R were dimensionally scaled to fit the size of the anole, using the known FP area from the segmentation. For example: the dimensions of an object (x) and mass (m) scale as $m \sim x^3$, thus $M \sim 1/x$. Since the FP area (A_{anole}^{FP}) is known from the segmentation, the following scaling rule for the acoustical mass of the anole is found $M_{anole} = \sqrt{A_{ostrich}^{FP}/A_{anole}^{FP}}\, M_{ostrich}$, with $A_{ostrich}^{FP}$ the ostrich FP area and $M_{ostrich}$ the effective acoustical mass of the ostrich cochlea on the medial FP surface. Similar derivations (see Muyshondt et al. (2016a)) lead to the following scaling rules: $K_{anole} = (A_{ostrich}^{FP}/A_{anole}^{FP})^{\frac{3}{2}} K_{ostrich}$ and $R_{anole} = (A_{ostrich}^{FP}/A_{anole}^{FP})R_{ostrich}$. The values for the anole were found to be $K = 43.35 \times 10^{12}$ Pa/m^3, $M = 3.916 \times 10^6$ Pa.s^2/m^3 and $R = 56.65 \times 10^9$ Pa.s/m^3. Finally, the pressure (P) on the FP resulting from the IE fluids in the scala vestibuli was related to Z_{IE} as follows: $P = Z_{IE} \cdot U_{FP}$, with U_{FP} the FP volume velocity. As the pressure in the model only depends on the FP volume velocity, the IE load only includes the reaction of the cochlear fluid to FP piston-like motion. The small but considerable IE pressure that arises from FP rocking motion (Dobrev et al., 2018) was therefore not considered. The estimated values of the IE load in the anole predict a more dominant stiffness than damping below 100 Hz. However, for the fluid-filled IE, it is the damping term which one expects to be dominant. In our models, IE loading only altered the ME response above 2 kHz (see Fig. 4), where it is indeed the damping (and inertia) which determine the amplitude of Z_{IE}. A dominant IE damping term agrees with the assumptions in a work by Hemilä et al. (1995), where it was shown that the mammalian IE acoustic impedance scales isometrically with TM area, FP area, the lengths of both lever arms, and the cubic roots of the ossicular masses. Since only the FP area was reported in Muyshondt et al. (2016a), scaling was done using the FP areas of the ostrich and the anole. Our scaling procedure assumes that K and M also scale with FP size and that the scaling itself also holds for non-mammals.

2.2.3 The coupled ME model

In the model, the acoustic pressure in the interaural cavity connected both MEs, acoustically coupling both MEs. Since the head of the anole is small in comparison to the wavelength of the sound waves in the relevant audible frequency range, the ILD of the sound on the TMs by the acoustic shadow of the head was neglected (Fletcher, 1992; Christensen-Dalsgaard and Manley, 2008; more explanation is given in the discussion). Therefore, the pressure input at both TMs had the same pressure amplitude P, but a phase difference $\Delta\varphi$ was incorporated to model the difference in travel time of the free-field pressure wave between the ears, depending on the location of the external sound source. Following Fletcher (1992), we applied homogeneous pressures $P_{\pm}$ at TM_1 $(+)$ and TM_2 $(-)$, separated by an interaural distance d as:

$$P_{\pm} = P \cdot \exp\left(\pm\frac{i\Delta\varphi}{2}\right) \cdot \exp(i\omega t) \quad ; \quad \Delta\varphi = \omega \cdot d \cdot \frac{\sin(\theta)}{c},$$

with i the imaginary unit, c the speed of sound, ω the angular frequency and θ the sound-source incident angle in the azimuthal (dorsal) plane with respect to the dorsoventral axis of the animal. Knowledge about the acoustics of the interaural cavity is sparse. In the present model, the cavity wall was modeled as a sound-hard boundary complying with $\boldsymbol{n} \cdot (\nabla P/\rho) = 0$, meaning that no pressure gradient (∇P) can exist normal ($\boldsymbol{n}$) to the wall, i.e., the wall reflects all sound pressures for a medium with density ρ. Segmentation of large datasets is a time-consuming process. We chose to only segment one half of the head and by using a mirroring operation we could construct a closed surface model of the entire coupled ME system including all the relevant structures. To make sure that the mirroring operation was done correctly, we segmented the contralateral TM and orientated the mirror plane in such a way that the mirrored version of the original TM coincided with the segmented contralateral TM. Furthermore, the interaural cavity primarily has to capture the acoustic propagation of the sound wave created by the TM vibration. The average edge length of the cavity mesh was 150 µm, enabling faster computation of the solution, while preserving the geometry of the interaural cavity. A convergence analysis showed that finer mesh sizes altered the solution less than 1%. In comparison, to obtain similar convergence with respect to the resolution of the mesh in the individual ME model, the average edge length of the ME mesh was required to be 50 µm.

3 Results

3.1 The isolated ME model

From the segmentation, we calculated a TM surface area of 3.34 mm^2 with an average thickness of 28.0 µm (see Fig. 2). The FP surface area was 0.141 mm^2. The TM-to-FP surface area ratio was thus 23.7, which is similar to the values reported in lizards having the same ME structure (Saunders et al., 2000). Given the location of the extracolumella attachment to the TM (see Fig. 1B), the ossicular lever or velocity ratio is expected to be around 2. The distance between the TM apices (d) was 7.68 mm and the cavity volume was 0.0597 cm^3, similar to previously reported values for the anole (Christensen-Dalsgaard and Manley, 2008). In Muyshondt et al. (2016b) a sensitivity analysis on the single-ossicle ear of the duck showed that the Young's modulus of the TM (E_{TM}) has the highest influence on the TM vibration response, while other parameters have negligible effects or enter through parameter interactions with the TM. The resonance frequency range of the TM of the anole lies between 3-4.5 kHz (Christensen-Dalsgaard and Manley, 2008). While varying material values, we observed a similar large influence of the TM's Young's modulus and using a value of 4 MPa allowed optimal correspondence of the model frequency range to the expected range.

Figure 3A shows the ME velocity levels between -30 and 12 dB [re. 1 mm/s/Pa] of our model with and without IE loading, using the parameters of Table 1. The TM velocities (solid lines) are measured at the distal end of the PI on the TM apex. The corresponding FP vibration velocities are also shown (dotted lines), and lie below the TM levels. In both the IE loaded (blue) and unloaded (red) models, the TM apex shows rapid fluctuations with lower vibration amplitudes beyond the resonance frequency of 3.7 kHz. As expected, IE loading (blue curve) lowers the maximal vibration amplitudes, and mainly influences mid to high frequencies. The phases in Fig. 3B show the typical $\pi/2$ phase difference of the PI with respect to the driving force under 2 kHz. At resonance the 180-degree phase transition occurs, while the fluctuations of the phases above the resonance frequency are signs of subsequent resonances and anti-resonances in the system. Beyond the first resonance, we also notice an increasing phase lag between the FP and PI, indicating a change in vibration mode of the extracolumella. The model with IE loading has the largest change of vibrational phase of the PI. Fig. 3C shows the velocity ratios, which give insight in the lever action of the ME. As anatomically predicted, at low frequencies we obtain a constant ratio of around 2. Above the TM resonance frequency, the TM vibrational patterns become more complicated (see also Fig. 3D) and thus the velocity ratio starts to fluctuate more rapidly. For the unloaded model the lever ratio seems to decrease, while the loaded model shows an increase in lever ratio. Both indicate a loss in proper impedance matching of the ME.

To visualize how the ME transfers acoustical energy from the TM to the FP, we refer to Fig. 3D. The color scale gives the velocity amplitudes of the ossicular chain at 250, 3600 and 8000 Hz (without IE loading). For any frequency it can be seen that the PI velocity is higher than the FP velocity. The PI velocity decreases from the distal end at the TM apex towards the proximal end at the connection with the extracolumella. The vibrational modes of the TM are illustrated in greyscale and show the increasingly complicated vibrational patterns at higher frequencies, which explains why the velocity ratios start to fluctuate (Fig. 3C). Experimental data on other species indicate that a rocking motion of the FP is present at higher frequencies (e.g., in birds (Muyshondt et al., 2018)). The precise type of FP motion is influenced by the (piston- and rocking-like) load of the IE fluid, which will also have some effect the total ME response (see section 2.2.2). In both the unloaded and loaded model, no significant rocking motion of the FP could be observed.

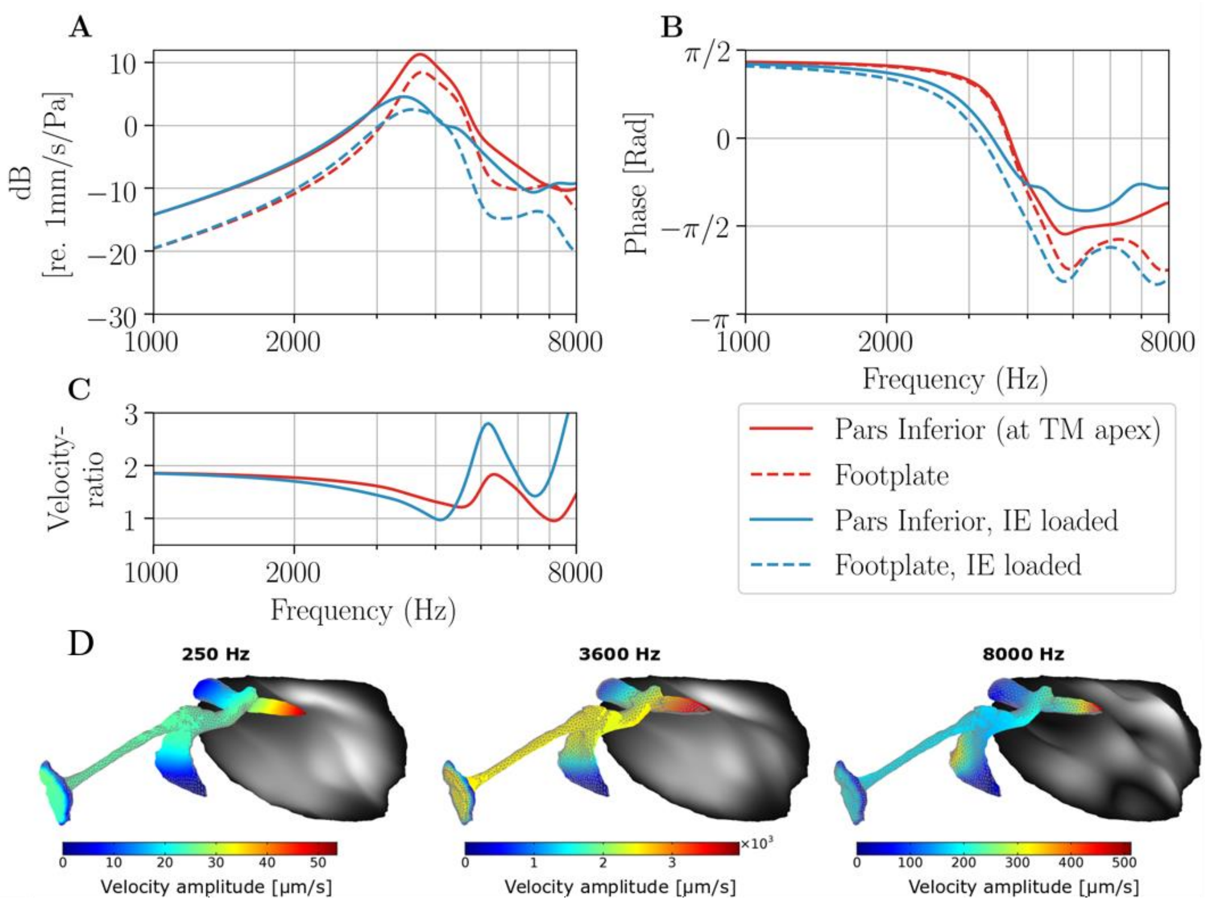

Figure 3. PI and FP response of the loaded and unloaded ME system with the material parameter values of Table 1. (A) velocity levels normalized to an incident pressure of 1 Pa (94 dB SPL), (B) velocity phases, and (C) velocity ratios of the PI and FP as a function of frequency. The PI vibration is evaluated at its distal end on the TM apex. (D) ME vibration amplitudes for low (250 Hz), mid (3600 Hz) and high (8000 Hz) frequencies within the hearing range of the anole, without IE loading on the FP. Corresponding vibrational modes of the TM are shown in greyscale.

3.2 *The coupled ME model*

After investigating the model of the individual ME, we focused on the model of the MEs coupled by the interaural cavity. In Fig. 4 we compare the vibrational response of the TM of the anole in our models to the experimental data of Christensen-Dalsgaard and Manley (2008). They measured TM vibration under free-field stimulation of 80 to 90 dB SPL in an anechoic room with the source at a distance of 1 m from the animal. The TM at the same side of the sound source is termed the ipsilateral (IL) TM, while the TM on the opposite side of the head is called the contralateral (CL) TM. As seen in Fig. 4A, the velocity of the IL TM was considerably higher than the CL TM within the considered frequency range. Although IL and CL vibrational patterns show great similarity for the three samples, there is some individual variation, especially for the CL TM response. In Fig. 4B we show the mean curve (black) of IL (solid) and CL (dot-dashed) data from Fig. 4A together with our model results, both for the models without (red) and with (blue) cochlear load. Low- (< 2.5 kHz) and high-frequency (> 5.5 kHz) velocity amplitudes differ the most with the experimental data when looking at the IL response, but the CL TM response approaches the experimental data with deviations of maximally 5 dB in these frequency regions. Most notably is that in these frequency ranges the models show a negligible difference between the IL or CL velocity amplitude, while the experiments do indicate directionality. The highest directionality is found between 3-4.5 kHz for both models, but the loaded model shows velocity levels that better agree with the experiments than the unloaded model. In the loaded model, TM velocity level differences between the IL and CL directions also extend over a broader frequency range.

Before discussing the results of the full field stimulation under different incident angles of the sound source, some conventions for visualization are explained. The results of the FE calculations with the coupled ME model in function of frequency and incident angle are presented as *cylindrical surface plots* (Christensen-Dalsgaard, 2011; Christensen-Dalsgaard and Manley, 2008) (see Fig 5). On the horizontal axis, the sound-source incident angle (θ) is given, while the vertical axis represents the sound-source frequency ($\omega/2\pi$). Horizontal lines in the surface plots of Fig. 5 correspond with polar plots around the head at a certain frequency, and vertical lines represent the TM frequency response function at a certain incident angle. Positive angles correspond with rotation to the IL side. TM velocities are evaluated at the TM apex (on the distal PI end) and reported in velocity levels (dB [re. 1 mm/s/Pa]) by using a color scale. To get an idea of ear directionality, a useful measure is the ratio of the TM velocity response relative to the 0-deg. midline, i.e. the frontal-caudal axis, as it indicates the level difference between the vibrations of the ipsilateral and contralateral TM. We follow the convention that velocity ratios need to be larger than 3 dB (Christensen-Dalsgaard, 2011) before useful directionality can be concluded. By using this criterion, we can also determine the directional bandwidth for which the criterion holds. Additionally, we present the phase differences with respect to the 0-deg midline, so both the generated level differences and phase differences can be assessed.

Fig. 5A shows the resulting vibration levels, which range between -17 and 12 dB [re. 1 mm/s/Pa] and become maximal between 3.5-5 kHz. At 90-deg. incidence we stimulate the IL ear, which explains why the maximal 12-dB velocity level is found here. The dashed lines at $\pm$90 deg. incidence correspond to the curves of Fig. 4B. When we compare the frequency response at different incident angles, we observe that the maximal velocity level consistently occurs around 4 kHz. At -90 deg. the source is on the other side of the animal's head and as expected this results in the lowest response for this TM. For low frequencies (<1.5 kHz) the wavelengths become much larger than the head size of the anole, so the resulting sound pressures on both TMs are practically the same in amplitude and phase, independent of the incident angle, and hence the θ dependence vanishes. Fig. 5B shows the velocity ratios relative to the 0-deg. midline. We find pronounced directionality of maximally ± 11 dB at the ± 90-deg. angles. The directional bandwidth is 1.5 kHz, although most of the level difference is concentrated between 3-4 kHz. Fig. 5C shows the corresponding phase differences, which range between -1.1 and 1.1 rad. The phase differences increase up until around 3 kHz, after which they quickly drop to zero near the resonance frequency. Around 5.5 kHz the phase differences seem to increase again, but this difference is smaller than the externally applied phase difference $\Delta\varphi$ due to the difference in travel time of the incident sound wave around the head. $\Delta\varphi$ rises linearly with frequency (see sect. 2.2.3), so above the resonance frequency no gained phase difference will be usable for the animal.

The effect of IE loading can be seen in the second row of Fig. 5. Although the velocity level decreases in Fig. 5D, qualitatively the same TM response as in Fig. 5A is observed. The behavior under and above the resonance frequency is preserved, but around the resonance the original maximum separates into two less-pronounced maxima, possibly a result of the IE load. The most interesting result is seen in Figure 5E. IE loading results in velocity ratios of ± 6 dB; the directional bandwidth however increases to 1.7 kHz. Although the bandwidth of Fig. 5B and 5E only differs by 0.2 kHz, it is interesting to see that IE loading creates plateaus of good directionality, in contrast to Fig. 5B where most of the dB difference was concentrated in a 1-kHz band. The more gradual decrease of the phase difference in Fig. 5F is consistent with this observation, since the damping term also leads to a less sharp phase drop-off at resonance. The maximal phase values of Fig. 5C and 5F differed by 0.2 rad.

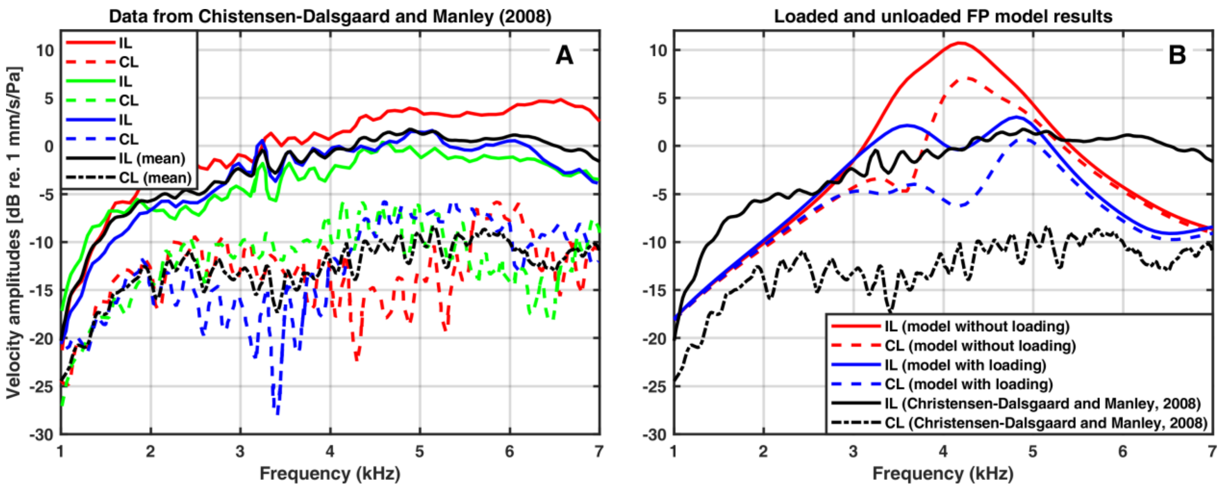

Figure 4. (A) Measured individual and averaged transfer functions of the ipsilateral (IL) and contralateral (CL) TM normalized to a free-field sound incidence of 1 Pa (i.e. 94 dB SPL). Data adapted from Christensen-Dalsgaard and Manley (2008). (B) Comparison of the mean curve of the experimental data (black) of the IL (solid) and CL (dot-dashed) TM to the model results for a loaded (blue) and unloaded (red) FP.

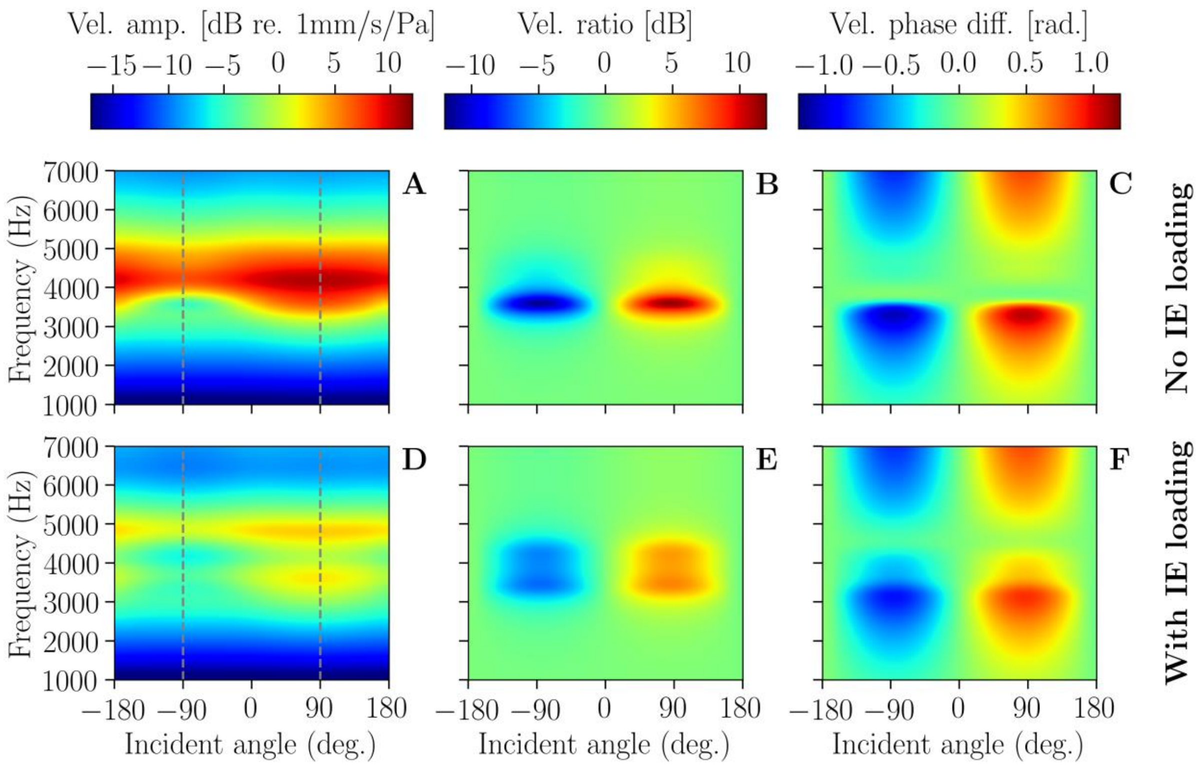

Figure 5. Results of the internally coupled ME model with (top row) and without (bottom row) IE loading. (A) IL TM vibration amplitude for different incident angels and frequencies. The velocity ratio relative to the 0-deg. midline gives an indication of the directionality. Both the level (B) and the phases (C) differences are shown. The bottom row (D-F) includes the effect of IE loading as described in sect. 2.2.2. Dotted lines (A&D) correspond to the model data shown in Fig. 4B.

4 Discussion

4.1 *The isolated ME model*

As seen in Table 1, most values in the models were taken from literature. Experimental data of the transfer function of the TM of the anole indicates resonances between 3-4.5 kHz (Christensen-Dalsgaard and Manley, 2008). A value of 4 MPa for the elasticity of the TM was adopted, since it resulted in a resonance frequency of 3.7 kHz of the TM (see Fig. 3A). The relatively low value of 4 MPa reflects the observation of Christensen-Dalsgaard and Manley (2008) that the TM of the anole is delicate. Isotropic values of TM Young's moduli in human are reported to be around 20 MPa (Volandri et al., 2011), while annular ligament elastic moduli are reported to be 1 MPa (Kwacz et al., 2015). Our model found values of 4 MPa and 0.145 MPa to be the most realistic for the anole. This indicates a ratio of 27.6 of TM-to-annular ligament elasticity in the anole, which is close to the ratio of 20 in humans under the assumption that Young's moduli are isotropic. Fig. 3C showed the PI-to-FP velocity (or lever) ratio. This ratio stays constant over a large part of the frequency range, while after the TM resonance oscillations start to occur. For the dragon lizard (*Amphibolorus retuculata*) the ME organization is similar to the anole and the extracolumella attaches at approximately 1/5 of the total PI+PS length, resulting in a lever ratio of 5 as reported in Saunders and Johnstone (1972). For the anole our models are thus consistent with these anatomical arguments (see Fig. 1A and Fig. 1B), because a ratio of 2 found in the model agrees with the anatomical relations. Similar lever ratios are found in other species (e.g., birds (Rosowski, 2013) and mammals (Hemilä et al., 1995, see Fig. 2B)), indicating that these ratios are well adapted for the lever function of the ME. As mentioned, both the loaded and unloaded model show no clear rocking motion of the FP, as the displacement patterns of the FP are largely uniform (Fig. 3D). However, measurements on other animals indicate that a rocking motion of the FP occurs at higher frequencies (e.g., Sim et al., 2010; Muyshondt et al., 2018). Flexion between the columella and extracolumella and flexion of the PI can reduce the FP response, and the extent and frequency range of this flexion may depend on the IE impedance (Manley, 1972). Measurements of anole FP movement and IE impedance could be a valuable addition to the current model and improve the current parameter- and literature-based IE impedance and FP motion.

4.2 *The coupled ME model*

Before model results are discussed, a more thorough explanation is given on why the ILD by the acoustic shadow of the head could be neglected in the anole of this study. The ILD on the TM between both sides becomes significant when the head of the animal and the wavelengths of sound become of the same size. A useful estimate can be made by considering the product $ka = 1$, with k the wavenumber and a the radius of a sphere, if the surface on which the sound falls in is approximated as a sphere. For small lizards, the distance between the TMs is about

1 cm. Using $k = \omega/c$, with ω the angular frequency and c the speed of sound in air, we find that $ka = 1$ equates to 5.4 kHz. If we take the classical problem of a plane sound wave reflecting off a sphere, it can be calculated that for this frequency the maximal pressure difference between the TMs never exceeds 2 dB SPL, precluding good directionality as the 3 dB threshold to localize a sound source (Christensen-Dalsgaard and Manley, 2005) is not met. On $ka = 2$ one finds maximal differences of 4.4 dB, but the corresponding frequency of 10.8 kHz is beyond the uppermost audible frequencies of most lizards, geckos being a notable exception (Manley and Kraus, 2010). Christensen-Dalsgaard and Manley (2008) mention that the TM response is asymmetrical over the midline (left-right) of the animal, but largely symmetrical over the interaural axis (front-back). For the anole, these data indicate that the size of the body is still sufficiently small compared to the wavelength of sound in the measured frequency range. Therefore, modeling the input pressures at both TMs with constant amplitude will adequately approximate the input pressures of real life conditions.

Our coupled model, and especially the model with cochlear loading, corresponded well with the experimental data of Christensen-Dalsgaard and Manley (2008) between 3–5 kHz when looking at IL TM vibration, but did not adequately describe directionality at the low and high frequencies (see Fig. 4). For the unloaded model the vibrational amplitudes at resonance exceed the estimated air particle velocity levels of 7.6 dB [re. 1 mm/s] at the input pressure of 94 dB SPL (i.e. 1 Pa). As seen in Fig. 4B, inclusion of cochlear loading allows for more realistic velocity amplitudes of the TMs at resonance, since the transfer function does not exceed the physical upper limit of 7.6 dB. The electrical analog model of Christensen-Dalsgaard and Manley (2008, Fig. 6C) shows a similar overestimation of the possible velocity levels of the TM. The CL TM response is overestimated in both the loaded and unloaded models, as experiments show that much lower velocity levels are present in nature, which results in larger directionality (see Fig. 4B). Directionality is found to encompass several kHz in many species, contrary to hearing at very specific frequencies. Therefore, it is reasonable that the loaded model better matches with the experimental data, since it allows for a broader system response. IL TM velocity for the loaded model within 3-5 kHz agrees well with experimental data and therefore emphasizes the need for incorporating IE loading in ME modeling. A possible explanation for the low frequency mismatch between model and experiment could be a result of the segmentation process. Without the nares and passages to the lungs segmented, our model cavity was a closed volume. This results in a smaller effective cavity volume, which enlarges the acoustic impedance of the enclosed volume of air. This higher cavity impedance could hinder the internal sound wave reaching the CL ear at the medial side with significant amplitude, especially for low frequencies, which diminishes directionality. In the experiments of Christensen-Dalsgaard and Manley (2008) directivity was abolished when blocking the CL TM with a dome of

Vaseline. Additionally, they blocked one nare (to not obstruct breathing), which reduced directionality with 2 dB and mostly below 2 kHz. If both nares and the airway to the lungs could have been blocked, the effect would have been larger, which may partially explain the higher CL TM velocity amplitudes in our model. The lumped-parameter models of Fletcher (1992) indicate similar effects of directionality with respect to open or closed nares. It was found that absolute directionality is lower with open nares, but that this lower sensitivity was compensated with a significant increase of the directional bandwidth, especially for low frequencies. The IL TM response on the contrary was lower in the FE model than in the experiments, both for low and high frequencies. For the low frequencies, this may be explained by (a) the value of the isotropic TM Young's modulus in the model or (b) the lack of knowledge on the fiber arrangements of the TM. The latter may also be of importance to explain the high-frequency deviations, since in humans the combination of the fiber arrangement and the asymmetrical placement of the malleus generates mistuned resonances to maximize energy transfer over a broad frequency spectrum (Fay et al., 2006). For lizards and birds, this fibrous middle layer is also present, but the fibers are generally less organized than in humans (Rosowski, 2013). Fig. 4B showed that IE loading broadens the directionality, but two distinct peaks seem to appear. It can be seen that the CL TM already shows separation into one large and one small peak, even without IE loading. The addition of the IE load Z_{IE} amplifies this distinction, since the IL TM response seems to separate into two peaks (at 3.5 kHz and 4.8 kHz) and the CL response separates even more. This separation was not present in Fig. 3A, which indicates that it is most likely a consequence of the load of the air in the cavity on the medial TM surface and the applied phase difference $\Delta\varphi$.

Fig. 5A and Fig. 5D showed TM velocity levels between -17 and 12 dB [re 1 mm/s/Pa]. Experiments on the anole reported TM velocity levels between -30 and 5 dB (Christensen-Dalsgaard and Manley, 2008), with a similar TM response as in Fig. 5A and 5D. In the experiments they started measuring from a lower frequency than presented here, which explains the difference in lower bound of the velocity level between model and experiment (see also Fig. 4B, where it can be seen that model and experimental IL curves are similar at low frequencies). Fig. 5B and Fig. 5E showed that velocity ratios of respectively ± 12 dB or ± 6 dB are possible, respectively. When we compare the velocity ratios of the FE model in Fig. 5B and Fig. 5E to experimental data (Christensen-Dalsgaard and Manley, 2008), they appear to underestimate the experimentally determined directional capabilities of the anole. In Christensen-Dalsgaard and Manley (2008), ratios between -30 and 30 dB are reported over a more than 6-kHz-wide frequency band. One resemblance with the reference data is that these ratios are relatively constant over a certain frequency range. Comparing the models without and with IE load, it is clear that the IE-loaded model creates these plateaus, at least up to about 5 kHz. This suggests that IE loading not only influences sound perception but also plays a role in sound localization. However, the directionality observed above 5 kHz is not predicted by the model. As noted in the previous paragraph several aspects could be the cause of these deviations, which requires a more detailed investigation of the anole's ME anatomy and material properties.

The phase differences (Fig. 5C and Fig. 5E) showed that the TM vibration phases could differ ± 1 radians at resonance (3.5 kHz). To the best knowledge of the authors, no phases have been reported in the literature of the coupled ME response in the anole. Alternatively, interaural amplitude and phase gain curves of the anole have been measured (Christensen-Dalsgaard and Manley, 2008), which represent the ratio of the TM transfer functions of local contralateral to local ipsilateral stimulation. To obtain these curves experimentally, they measured the response of one TM due to local stimulation of the same ear and the opposite ear. Without the interaural cavity connecting the MEs, such experiments would yield no displacement of the TM under local contralateral stimulation. This resulted in a gain of the amplitude and a shift of the phase in the ratios of the TM transfer functions. These experiments reported phase gains with a linear slope of -0.4 rad/kHz below resonance and a slope of -1.1 rad/kHz above resonance. Our results with IE loading (Fig. 5F) of the phase difference with stimulation of both TMs indicate a slope of 0.5 rad/kHz below resonance and a slope of -1.3 rad/kHz above resonance. The externally applied phase difference $\Delta\varphi$ at 3.5 kHz for 90 deg. incidence is 0.44 rad, while the model with IE loading predicts phase differences of 0.8 rad. The interaural connection therefore seems to double the "effective distance" between both ears (from 7 mm to 14 mm), which was also experimentally reported in the phase gain curves of Christensen-Dalsgaard and Manley (2008).

The work of Vossen et al. (2010) and Vedurmudi et al. (2016a, 2016b) investigated interaural coupling by modeling each TM as a circular membrane, coupled by an air-filled cylinder. TM vibrations were analytically calculated under certain assumptions. It was shown that the fundamental TM frequency separates the directionality into two regions. Below the fundamental frequency of the TM the phase differences were the dominant cues, while above the TM resonance frequency the velocity ratios were dominant. Fig. 5B and 5E show that the same conclusions hold in our models. The phase differences rise gradually up until the resonance frequency, but drop off rather abruptly above the TM resonance frequency. The level differences only become relevant around and above the resonance frequency, and then either drop off quickly (no IE loading, Fig. 4B and Fig. 5B) or show local plateaus (with IE loading, Fig. 4B and Fig 5E). Since our model uses the exact anatomy of the coupled ear system of the animal, we have greater modeling freedom to investigate the effect of all individual ME components compared to the referenced work. The model of Vedurmudi et al. (2016a, 2016b) shows the greatest resemblance to Fig. 5B-C (without IE loading) rather than Fig. 5E-F (with IE loading). We noted that including IE loading leads to a better agreement with the experimental data from Christensen-Dalsgaard and Manley (2008). Therefore, we predict that in reality a more gradual transition between the two regions above and below TM resonance will occur (see Fig. 5E-F) than what current analytical models predict.

5 Conclusion

In this study we presented the first anatomically accurate model of interaural coupling in the brown anole (*Anolis sagrei*), using FE modeling. We found that a Young's modulus of 4 MPa for the TM and 0.145 MPa for the annular ligament described the ME response of the anole most adequately. This resulted in a lever ratio of around 2 between the input and output of the ME, which was in accordance with anatomical relations of the ME and was consistent with the literature. The coupled model of the MEs of the anole and the interaural cavity showed that maximal velocity ratios of ± 12 dB and phase differences of ± 1.1 rad are possible between the TMs. With IE loading these values became ± 6 dB and ± 0.9 rad, respectively, but with broader plateaus of directionality. The phase differences between the TMs in the model show that the interaural cavity makes the head of the anole appear at least twice as large compared to what the external phase differences predict. IE loading plays not only a role in sound perception but also in sound-source localization. The velocity amplitude ratios and phase differences without IE loading seem to be separated into two distinct regions of localization cues around the TM resonance frequency. When IE loading is included, the transition from low-frequency phase cues to higher-frequency level cues becomes more gradual, which expands on the previous analytical models of interaural coupling in the literature.

Declaration of interest

None.

Contributors

P.L. created the FE model, analyzed the data and wrote the manuscript. P.G.G.M. contributed to the writing of the manuscript. P.G.G.M. and J.J.J.D. participated in the design of the study. All authors gave their final approval for publication.

Acknowledgments

The authors want to thank Dr. J. Goyens for performing the µCT scans and the reviewers for their valuable comments and suggestions on the manuscript. This work was financed by the Research Foundation – Flanders (FWO), grant nr. 11D4319N and 11T9318N.

References

Brittan-Powell, E.F., Christensen-Dalsgaard, J., Tang, Y., Carr, C., Dooling, R.J., 2010. The auditory brainstem response in two lizard species. J. Acoust. Soc. Am. 128, 787–794.

Buytaert, J., Goyens, J., De Greef, D., Aerts, P., Dirckx, J., 2014. Volume shrinkage of bone, brain and muscle tissue in sample preparation for micro-CT and light sheet fluorescence microscopy (LSFM). Microsc. Microanal. 20, 1208–1217.

Christensen-Dalsgaard, J., 2011. Vertebrate pressure-gradient receivers. Hear. Res. 273, 37–45.

Christensen-Dalsgaard, J., Manley, G.A., 2005. Directionality of the lizard ear. J. Exp. Biol. 208, 1209–1217.

Christensen-Dalsgaard, J., Manley, G.A., 2008. Acoustical coupling of lizard eardrums. JARO 9, 407-416.

Dobrev, I., Schär, M., Chatzimichalis, M., Prochazka, L., Pfiffner, F., Röösli, C., Huber, A.M., Sim, J.H. Intracochlear pressure change by the 3D motion components of the stapes [abstract]. In: Abstract Book of the 8th International Symposium on Middle-Ear Mechanics in Research and Otology; July 5–9, 2018; Shanghai, China; pp. 115–116.

Dooling, R., Loch, B., Dent, M., 2000. Hearing in birds and reptiles. In: Dooling, R.J., Fay, R.R., Popper, A.N. (Eds.), Comparative Hearing: Birds and Reptiles. Springer, New York, NY, pp. 308–347.

Fay, J.P., Puria, S., Steele, C.R., 2006. The discordant eardrum. PNAS 103, 19743–19748.

Fletcher, N.H., 1992. Low-frequency auditory models. In: Fletcher, N.H. (Ed.), Acoustic Systems in Biology. Oxford University Press, p. 154.

Grothe, B., Pecka, M., 2014. The natural history of sound localization in mammals-a story of neuronal inhibition. Front. Neural Circuit. 8, 116.

Hemilä, S., Nummela, S., Reuter, T., 1995. What middle ear parameters tell about impedance matching and high frequency hearing. Hear. Res. 85, 31–44.

Koike, T. & Wada, H., Kobayashi, T., 2001. Effect of depth of conical-shaped tympanic membrane on middle-ear sound transmission. JSME Int. J. Ser. C 44, 1097–1102.

Köppl, C., 2009. Evolution of sound localisation in land vertebrates. Curr. biol. 19, 635–639.

Kwacz, M., Rymuza, Z., Michałowski, M., Wysocki, J., 2015. Elastic properties of the annular ligament of the human stapes–AFM measurement. J. Assoc. Res. Otolaryngol. 16, 433–446.

Manley, G.A., 1972. Frequency response of the middle ear of geckos. J. Comp. Physiol. 81, 251–258.

Manley, G.A., 2010. An evolutionary perspective on middle ears. Hear. Res. 263, 3–8.

Manley, G.A., 2017. The Cochlea: What it is, where it came from, and what is special about it. In: Manley, G.A., Fay, R.R., Popper, A.N., Understanding the Cochlea. New York: Springer Science, pp. 17–32.

Manley, G.A., Köppl, C., 1998. Phylogenetic development of the cochlea and its innervation. Curr. Opin. Neurobiol. 8, 468–474.

Manley, G.A., Kraus, J.E.M., 2010. Exceptional high-frequency hearing and matched vocalizations in Australian pygopod geckos. J. Exp. Biol. 213, 1876–1885.

Mason, M.J., Farr, M.R.B., 2013. Flexibility within the middle ears of vertebrates. JARO 127, 2–14.

Muyshondt, P.G.G., Aerts, P., Dirckx, J.J.J., 2016a. Acoustic input impedance of the avian inner ear measured in ostrich (Struthio camelus). Hear. Res. 339, 175–183.

Muyshondt, P.G.G., Claes, R., Aerts, P., Dirckx, J.J.J., 2018. Quasi-static and dynamic motions of the columellar footplate in ostrich (Struthio camelus) measured ex-vivo. Hear. Res. 357, 10–24.

Muyshondt, P.G.G., Soons, J.A.M., De Greef, D., Pires, F., Aerts, P., Dirckx, J.J.J., 2016b. A single-ossicle ear: Acoustic response and mechanical properties measured in duck. Hear. Res. 340, 35–42.

Rosowski, J.J., 2013. Comparative middle ear structure and function in vertebrates, In: Puria, S., Fay, R.R., Popper, A.N. (Eds.), The Middle Ear: Science, Otosurgery, and Technology, Springer Handbook of Auditory Research. Springer, New York, NY, pp. 31–65.

Saunders, J.C., Duncan, R.K., Doan, D.E., Werner, Y.L., 2000. The middle ear of reptiles and birds. In: Dooling, R.J., Fay, R.R. , Popper, A.N., Comparative Hearing: Birds and Reptiles. Springer, New York, NY, pp. 13–69.

Saunders, J.C., Johnstone, B.M., 1972. A comparative analysis of middle-ear function in non-mammalian vertebrates. Acta Otolaryngol. 73, 353–361.

Sim, J.H., Chatzimichalis, M., Lauxmann, M., Röösli, M., Eiber, A., Huber, A.M., 2010. Complex stapes motions in human ears. JARO 11, 329–341.

Thomassen, H.A., Gea, S., Maas, S., Bout, R.G., Dirckx, J.J.J., Decraemer, W.F., Povel, G.D.E., 2007. Do Swiftlets have an ear for echolocation? The functional morphology of Swiftlets' middle ears. Hear. Res. 225, 25–37.

Van der Jeught, S., Dirckx, J.J.J., Aerts, J.R.M., Bradu, A., Podoleanu, A.G., Buytaert, J.A.N., 2013. Full-field thickness distribution of human tympanic membrane obtained with optical coherence tomography. JARO 14, 483–493.

Vedurmudi, A.P., Goulet, J. Christensen-Dalsgaard, J., Young, B.A., Williams, R., van Hemmen, J.L., 2016a. How internally coupled ears generate temporal and amplitude cues for sound localization. Phys. Rev. Lett. 116, 028101.

Vedurmudi, A.P., Young, B.A., van Hemmen, J.L., 2016b. Internally coupled ears: mathematical structures and mechanisms underlying ICE. Biol. Cybern. 110, 359–382.

Volandri, G., Di Puccio, F., Forte, P., Carmignani, C., 2011. Biomechanics of the tympanic membrane. J. Biomech. 44, 1219–1236.

Voss, S.E., Nakajima, H.H., Huber, A.M., Shera, C.A., 2013. Function and acoustics of the normal and diseased middle ear, In: Puria, S., Fay, R.R., Popper, A.N. (Eds.), The Middle Ear: Science, Otosurgery, and Technology, Springer Handbook of Auditory Research. Springer, New York, NY, pp. 67–91.

Vossen, C., Christensen-Dalsgaard, J., van Hemmen, J.L., 2010. Analytical model of internally coupled ears. J. Acoust. Soc. Am. 128, 909–918.

Wever, E.G., 1978. The reptile ear: Its structure and function. Princeton University Press, Princeton, NJ.

Wever, E.G., Werner, Y.L., 1970. The function of the middle ear in lizards: Crotaphytus collaris (Iguanidae). J. Exp. Zool. 175, 327–341.

Young, B.A., 2016. Anatomical influences on internally coupled ears in reptiles. Biol. Cybern. 110, 255–261.